AIAA JOURNAL
Vol. 47, No. 11, November 2009

Combustion Analysis Using Roe's Scheme and the Spalart–Allmaras Model

T. Belmrabet*
École Militaire Polytechnique, Algiers, 16111 Algeria
M. Talice† and G. Delussu‡
Center for Advanced Studies, Research and Development in Sardinia, 09010 Pula, Italy
M. Mulas§
Karalit s.r.l. 09010 Pula, Italy
and
S. Hanchi¶
École Militaire Polytechnique, Algiers, 16111 Algeria.

DOI: 10.2514/1.44331

The present work describes an efficient computational method for the simulation of turbulent flames. The main three ingredients of the method are Roe's schemes, the Spalart–Allmaras one-equation turbulence model, and a general preconditioning technique. These three ingredients are well known to ensure accuracy, robustness, and generality. The solution of the conservation equations is fully coupled, and the method is implemented in a three-dimensional parallel implicit solver. This potentially allows the use of the same mathematical method for the analysis of turbulent reactive flows at all speeds. The choice of the Spalart–Allmaras model, as opposed to typical two-equation models requires particular attention on the derivation of the micromixing time. Such a derivation is of fundamental importance, for the micromixing time represents the base upon which chemical source terms are built for many combustion models. Deriving a correct model for the micromixing time from the only resolved turbulent quantity kinematic eddy viscosity is challenging. To test the method, two low-Mach-number (0.1–0.2) turbulent reactive flows are simulated using the eddy dissipation model, and the results are compared with both experiments and previous numerical studies. It is established that the proposed method leads to satisfactory results.

Nomenclature

A_{ebu}, B_{ebu}	=	eddy dissipation model coefficients
C_l, C_μ, A_ε	=	closure coefficients
C_p	=	specific heat at constant pressure, J/kg · K
D	=	mass diffusion coefficient, m^2/s
D_{kl}	=	binary mass diffusivity coefficient, m^2/s
$D_{T,k}$	=	effective thermal diffusion coefficient, m^2/s
$\mathbf{F}$	=	vector of the inviscid flux
$\mathbf{G}$	=	vector of the viscous flux
H	=	total sensible enthalpy of mixture, J/kg
h	=	sensible enthalpy of mixture, J/kg
h_k	=	sensible enthalpy of species k, J/kg
h_k^0	=	specific enthalpy of formation of species, J/kg
l_t	=	turbulent integral scale, m
l_ε	=	characteristic length scale, m
M	=	Jacobian matrix
M_k	=	molecular weight of species k, kg/kmol
M_m	=	modified Jacobian matrix
N	=	number of chemical species in the system
n_x, n_y, n_z	=	direction cosines
P	=	preconditioning matrix
Pr_t	=	turbulent Prandtl number
p	=	static pressure, Pa
$\mathbf{Q}$	=	vector of conservative variables
$\mathbf{Q}_v$	=	vector of viscous primitive variables
q	=	components of heat flux vector, W/m^2
R_g	=	universal gas constant, J/mol.K
R_{mix}	=	mixture specific gas constant, J/kg.K
Re_y	=	local turbulent Reynolds number
$\mathbf{S}$	=	vector of the sources terms
S	=	mean strain rate, 1/s
S_{ij}	=	rate of strain tensor, 1/s
Sc_t	=	turbulent Schmidt number
T	=	temperature, K
$T_{\text{ref},k}$	=	reference temperature for species, k, K
t	=	time, s
u, v, w	=	Cartesian component of velocities, m/s
V_n	=	normal velocity, m/s
V_p	=	local preconditioning velocity, m/s
x, y, z	=	Cartesian coordinates
Y	=	mass fraction
y^+	=	normalized wall distance
δ_{ij}	=	Kronecker's delta function
ε	=	dissipation rate of turbulent kinetic energy, m^2/s^3
κ	=	turbulent kinetic energy, m^2/s^2
λ	=	thermal conductivity or matrix eigenvalue, W/m · K
λ_ε	=	damping function
μ	=	dynamic viscosity, kg/m.s
ν	=	kinematic viscosity, m^2/s
$\tilde{\nu}$	=	Spalart–Allmaras transported variable, m^2/s
ν_t	=	kinematic eddy viscosity, m^2/s
$\nu'_{i,r}$	=	stoichiometric coefficient for the ith reactant in reaction r

Received 12 March 2009; revision received 29 June 2009; accepted for publication 30 June 2009.

*Researcher, Fluid Mechanics Laboratory, BP 17 Bordj El Bahri; toufik_belmrabet@yahoo.fr.

†Senior Researcher; Renewable Energy Group, Scientific And Technological Park; talice@crs4.it.

‡Expert Researcher, Renewable Energy Group, Scientific And Technological Park; surfer@crs4.it.

§President, Scientific And Technological Park; mulas@crs4.it. Member AIAA.

¶Professor, Fluid Mechanics Laboratory, BP 17 Bordj El Bahri; samir_hanchi@yahoo.fr.

$\nu''_{i,r}$ = stoichiometric coefficient for the product ith in reaction r
ρ = density, kg/m^3
τ_{ij} = viscous stress tensor, N/m^2
τ_t = turbulent mixing time scale, s
χ = mole fraction
Ω = vorticity, 1/s, cell's volume, m^3
ω = turbulent eddy frequency, 1/s
$\dot{\omega}$ = mass reaction rate, kg/m$^3 \cdot$ s

Subscripts

i, j, k = components in i, j, k directions
i, k, l = species
P = product
p = derivative with respect to pressure
R = reactant
r = reaction
SA = derived from Spalart–Allmaras model
T = derivative with respect to temperature
x, y, z = components in x, y, z directions
Y = derivative with respect to species mass fraction

Introduction

DURING the last few decades, a lot of work has been devoted to modeling turbulent combustion using computational fluid dynamics (CFD) with a variety of approaches and modeling techniques. In Reynolds averaged Navier–Stokes (RANS) formulations, which are still extensively used in practical industrial simulations, turbulent combustion models generally require knowledge of turbulent mixing time scale τ_t, estimated from the turbulent kinetic energy κ, and its dissipation rate ϵ. This is the main reason why turbulent combustion modeling is usually coupled with a κ–ϵ like turbulence model [1]. This is true not only for the eddy dissipation model (EDM), in which τ_t explicitly appears in the calculus of the mean reaction rate, but also for the majority of turbulent combustion models for premixed and nonpremixed flames. For example, in the framework of turbulent premixed flames modeling, turbulent time scale is required to compute the mean reaction rates in both the eddy break up model [2] and the Bray–Moss–Libby model [3,4]. For the majority of models that use the flame surface density and for which the mean reaction rate is described in term of flame surface area [5], the integral time scale is required to estimate the flame stretch induced by the turbulent flow. This is the case for the coherent flame models: CFM1, CFM2 a and CFM2 b [6], the Mantel–Borghi (MB) model [7], and the Cheng–Diringer (CD) model [8]. For those models that are based on statistical analysis a probability density function (PDF) is used instead. Two main approaches exist to estimate this function. In the first one, the shape of the PDF function is assumed to be known (presumed PDF). In the second approach, a balance equation for the PDF has to be solved. The PDF transport equation, rarely used in industrial simulations because of its computational cost, does not make explicit use of the turbulent time scale. It is still generally coupled with the κ–ϵ model. On the other hand, presumed PDF modeling is often used for industrial applications. Integral time scale is required in the closure of the additional transport equation for the progress variable variance [1].

As far as turbulent nonpremixed flames modeling is concerned, knowledge of the turbulent time scale is required for the three main ways used to address the turbulence chemistry closure problem; namely, turbulent mixing, geometrical, and statistical approaches. In fact the turbulent time scale is explicitly used in the EDM model in the closure of additional transport equations, for both the presumed PDFs and the flamelet model's approach (mixture fraction variance and mean scalar dissipation rate), as well as in the closure of the balance equation for the flame surface density [9] (estimation of the mean strain rate acting on the flame surface). More details on nonpremixed turbulent flames modeling can be found in [1,10].

The κ–ϵ model has some well-known drawbacks in the low Reynolds regime, especially in the walls' proximity. Other two-equations models have been developed using various combinations of κ and ϵ to derive alternative transport equations to overcome these problems (i.e., κ–ω models). One important advantage of the κ–ω model comparatively to the κ–ϵ model is the treatment of the near-wall region in boundary-layer flows [11], particularly for low Reynolds number flows. The turbulent mixing time is obtained directly from the inverse of turbulence frequency ω.

More recently, the SA one-equation turbulence model, presented in [12], has become very popular in the CFD community. The model presents several advantages with respect to both algebraic and two-equation models: firstly, it is "local" and therefore well suited to block-structured as well as unstructured Navier–Stokes codes. Secondly, it is easy to use, requires trivial boundary conditions, and shows no stiffness, which is a typical problem of two-equation κ–ϵ like models written in low Reynolds number formulations for the near-wall region. The model solves for a modified turbulent viscosity $\tilde{\nu}$ and it is constructed as three nested models: for free shear flows, for near-wall region and high Reynolds number (the log region of the boundary-layer), and for near-wall region and low Reynolds number, (which allows integration to the laminar viscous sublayer).

Depending on the mesh resolution near solid boundaries, the various nested models may become passive, and so no strict requirement exists on y^+. However, the main limitation of this model (and any other one-equation model) is that the mixing length (required for the estimation of the dissipation rate) must be fixed by the user. Indeed, for complex turbulent flows, it would be unreasonable to expect the mixing length to maintain the same value at every location in the flow field [13]. A possible solution to this problem, which makes use of a non constant mixing length, is presented in this work and tested against several test cases.

In more recent years, many efforts have been made to develop unified numerical approaches to solve a wider class of fluid flow problems [14]. For this purpose, either typical "incompressible" methods are generalized for high speed compressible flows, or vice versa, "compressible" methods are extended to low speed incompressible flows. The two methods are now more often called pressure- and density-based methods. The density-based approach has several advantages. Firstly, it would eliminate the inherent limitations of the pressure-based approach. Temperature and pressure regain, in fact, their role of being truly independent thermodynamic variables. This allows the possibility to numerically simulate situations in which surface heat transfer and pressure wave instabilities are of interest. Moreover, this mathematical framework would be ready for extending the combustion models (if needed) to cases of transonic and supersonic combustion. The proposed model is implemented in a 3-D parallel fully coupled density-based solver.

Mathematical Model

Governing Equations

Let us consider the unsteady multicomponent reacting flow system, which, in fully compressible, preconditioned, compact, three-dimensional vector form, written as

$$\frac{\partial \mathbf{Q}}{\partial t} + P \cdot \left[\frac{\partial (\mathbf{F}_x - \mathbf{G}_x)}{\partial x} + \frac{\partial (\mathbf{F}_y - \mathbf{G}_y)}{\partial y} + \frac{\partial (\mathbf{F}_z - \mathbf{G}_z)}{\partial z} \right] = P \cdot \mathbf{S} \tag{1}$$

where

$$\begin{aligned}
\mathbf{Q} &= (\rho \quad \rho u \quad \rho v \quad \rho w \quad \rho E \quad \rho Y_1 \quad \dots \quad \rho Y_{N-1})^T \\
\mathbf{F}_x &= (\rho u \quad \rho u^2 + p \quad \rho uv \quad \rho uw \quad \rho uH \quad \rho uY_1 \quad \dots \quad \rho uY_{N-1})^T \\
\mathbf{F}_y &= (\rho v \quad \rho uv \quad \rho v^2 + p \quad \rho vw \quad \rho vH \quad \rho vY_1 \quad \dots \quad \rho vY_{N-1})^T \\
\mathbf{F}_z &= (\rho w \quad \rho uw \quad \rho vw \quad \rho w^2 + p \quad \rho wH \quad \rho wY_1 \quad \dots \quad \rho wY_{N-1})^T
\end{aligned} \tag{2}$$

and

$$\mathbf{G}_x = (0 \;\; \tau_{xx} \;\; \tau_{xy} \;\; \tau_{xz} \;\; u\tau_{xx} + v\tau_{xy} + w\tau_{xz} + q_x \;\; \dot{m}_{1,x} \;\; \ldots \;\; \dot{m}_{N-1,x})^T$$
$$\mathbf{G}_y = (0 \;\; \tau_{xy} \;\; \tau_{yy} \;\; \tau_{yz} \;\; u\tau_{xy} + v\tau_{yy} + w\tau_{yz} + q_y \;\; \dot{m}_{1,y} \;\; \ldots \;\; \dot{m}_{N-1,y})^T$$
$$\mathbf{G}_z = (0 \;\; \tau_{xz} \;\; \tau_{zy} \;\; \tau_{zz} \;\; u\tau_{xz} + v\tau_{yz} + w\tau_{zz} + q_z \;\; \dot{m}_{1,z} \;\; \ldots \;\; \dot{m}_{N-1,z})^T$$
$$\mathbf{S} = (0 \;\; 0 \;\; 0 \;\; 0 \;\; 0 \;\; \dot{\omega}_1 \;\; \ldots \;\; \dot{\omega}_{N-1})^T \tag{3}$$

where

$$q_i = \lambda \frac{\partial T}{\partial x_i} + \sum_{k=1}^{N} \dot{m}_{k,i} h_k \qquad \dot{m}_{k,i} = \rho D_k \frac{\partial Y_k}{\partial x_i} + D_{T,k} \frac{\nabla T}{T}$$
$$\tau_{ij} = \mu \left(\frac{\partial u_i}{\partial x_j} + \frac{\partial u_j}{\partial x_i} \right) - \frac{2}{3} \mu \delta_{ij} + \frac{\partial u_k}{\partial x_k} \tag{4}$$

Assuming a mixture of thermally perfect gases, ρ, h_k, and h are modeled as

$$\rho = \frac{p}{R_{\text{mix}} T} \qquad R_{\text{mix}} = R_g \sum_{k=1}^{N} \frac{Y_k}{M_k} \qquad H = \sum_{k=1}^{N} Y_k h_k$$
$$h_k = \int_{T_{\text{ref},k}}^{T} C p_k \mathrm{d}T + h_k^0 \tag{5}$$

For each chemical species, Cp_k varies significantly with temperature and could be modeled as polynomial fits of static temperature, with coefficients taken from the JANNAF table. Values of μ_k and λ_k are obtained via kinetic theory, whereasD_{kl} values are computed via the Chapman–Enskog formula [15]. To compute mixture's viscosity and thermal conductivity Wilke's and Wassiljewa's formulas are applied. The effective molecular diffusion coefficient for each species is computed as

$$D_k = \frac{1 - \chi_k}{\sum\limits_{l \neq k} \left(\frac{\chi_l}{D_{kl}} \right)} \tag{6}$$

The matrix $\mathbf{P}$ in Eq. (1) is given by $P = M \cdot M_m^{-1}$. $\mathbf{M}$ is the Jacobian matrix of the conservative variables vector $\mathbf{Q}$ with respect to the vector of the viscous primitive variables $\mathbf{Q}_v = (p, \;\; u, \;\; v, \;\; w, T, Y_1, \ldots, Y_{N-1})^T$.

M_m is a modified version of $\mathbf{M}$. No modification brings back the original nonpreconditioned system ($P = I$). The matrix $\mathbf{M}$ contains arbitrary thermodynamics in terms of derivatives of density and enthalpy with respect to pressure, species mass fraction, and temperature (ρ_p, ρ_T, ρ_{Y_i}, h_p, h_T, h_{Y_i}); whereas the matrix M_m contains a modified thermodynamics in terms of ρ_p^m. The characteristic speed is obtained with the following choice of ρ_p^m [14]:

$$\rho_p^m = 1/V_p^2 - \rho T / \rho h_T \tag{7}$$

in which V_p plays a crucial role. It should be as low as possible but not smaller than any local transport velocity for stability considerations [14].

Numerical Scheme

Equations are integrated with a cell-centered finite volume method on block-structured meshes. Convective inviscid fluxes are computed by a second order Roe's scheme [16,17], based on the decomposition of the Euler equations in waves, so that proper upwinding can be applied to each wave depending on the sign of the corresponding wave's speed. This implies that the flux vector is written as

$$F^*_{i+1/2} = \frac{F_i + F_{i+1}}{2} - \frac{1}{2} [P^{-1} R_P |\Lambda_P| L_P]_{i+1/2} (\mathbf{Q}_{i+1} - \mathbf{Q}_i) \tag{8}$$

which represents the sum of a central part and a matrix dissipation part, computed at the cell interface, denoted by $i + 1/2$. R_P, and L_P represent the matrices of right and left eigenvectors of:

$$D_P = P \left(\frac{\partial \mathbf{F}_x}{\partial \mathbf{Q}} n_x + \frac{\partial \mathbf{F}_y}{\partial \mathbf{Q}} n_y + \frac{\partial \mathbf{F}_z}{\partial \mathbf{Q}} n_z \right) \tag{9}$$

and $|\Lambda_P|$ is the diagonal matrix whose elements are the absolute values of the eigenvalues of the system matrix D_P. Second-order accuracy is achieved by computing these elements using an appropriate limiter which assures monotonicity of the solution at discontinuities and at local minima and maxima [17]. The eigenvectors's expression in terms of conservative variables is rather complicated. Easier algebra and programming can be achieved by transforming Eq. (8) in the equivalent expression for the primitive variables $\mathbf{Q}_v$. The numerical flux evaluation scheme becomes:

$$F^*_{i+1/2} = \frac{F_i + F_{i+1}}{2} - \frac{1}{2} [M_m R_P^v |\Lambda_P| L_P^v]_{i+1/2} (\mathbf{Q}_{vi} - \mathbf{Q}_{vi}) \tag{10}$$

in which R_P^v and L_P^v are the right and left eigenvector matrices in primitive variables of the preconditioned Euler matrix $D_P^v = M^{-1} \cdot D_P \cdot M$. Equations (8) and (10) are equivalent: they both provide the fluxes (and so the residuals) for the conserved quantities (mass, momentum, mass fractions, and total energy per unit volume). Equation (8) is written in terms of conservative variables; Eq. (10) makes use of eigenvectors in primitive variables, allowing easier algebra and less intensive computational load. Viscous fluxes and source terms are calculated with standard cell-centered finite-volume techniques and they are both second-order accurate. The eigenvalues of the system, also elements of Λ_P in Eq. (10) are:

$$\lambda_1 = \lambda_2 = \lambda_3 = \lambda_6 = \lambda_7 = \lambda_{N+4} = V_n \tag{11}$$

$$\lambda_{4,5} = V_n \left(\frac{d + d^m}{2d^m} \right) \pm \sqrt{V_n^2 \left(\frac{d + d^m}{2d^m} \right)^2 + \frac{\rho h_T}{d^m}} \tag{12}$$

where

$$d = \rho \rho_p h_T + \rho_T (1 - \rho h_p)$$

and

$$V_n = u n_x + v n_y + w n_z$$

The value of d^m can be obtained from d by taking ρ_p^m instead of ρ_p.

Once written in finite-volume and semidiscrete forms, the system in Eq. (1) dropping superscripts, after linearization and rearrangement, becomes:

$$\left(M_m \frac{\Omega}{\Delta t} + \frac{\partial \text{RES}}{\partial \mathbf{Q}_v} \right) \Delta \mathbf{Q}_v = -\text{RES} \tag{13}$$

in which RES is the conservative variables' residuals vector and Ω the cell's volume. Updating is done in terms of the viscous primitive variables $\mathbf{Q}_v$; namely, pressure, temperature, velocity components, and the species mass fractions.

At each time step, linearization leads to a linear system which is to be solved by an iterative method (red-black relaxation scheme). When unconditional stability is achievable, Eq. (13) may become in principle a Newton method able to deliver quadratic convergence if the linear system solution is pushed till full convergence at each linearization step. In a typical implementation the Jacobian matrix of the residual vector is done using a shorter stencil (equivalent to first order scheme) leading to a quasi-Newton method when the numerical scheme can stand infinite Courant–Friedrich–Levy (CFL) number. The choice of the red-black relaxation scheme is motivated by the fact that it allows a straightforward parallelization without loss of convergence and computational efficiency.

Together with the CFL number, the global convergence properties of the method are determined by the convergence level chosen for the solution of the linear system (the number of sweeps of relaxation) as well as by the underrelaxation parameter.

Turbulence and Combustion Modeling

In this work, the SA turbulence model [12] is used to model the unresolved turbulent flow quantities. This model is a one-transport equation model for a modified kinematic eddy viscosity $\tilde{\nu}$. The model's differential equation is derived by "using empiricism and arguments of dimensional analysis, Galilean invariance and selected dependence on the molecular viscosity" [12]. It does not require any finer grid resolution than that needed to capture the velocity field gradients with algebraic models. A new set of damping functions [18] to fix the problem of negative production and a modification of the original model proposed by Dacles-Mariani et al. [19] to take into account the effect of the mean strain on the turbulence production have also been used in the present work. The model is solved with an implicit algorithm decoupled from the main transport equations. The solution algorithm is the same as the one described above [14].

Combustion is modeled via a two-step global reaction mechanism, by which production and combustion of carbon monoxide is taken into account:

$$2CH_4 + 3O_2 \Rightarrow 2CO + 4H_2O \tag{14}$$

$$2CO + O_2 \Rightarrow 2CO_2 \tag{15}$$

Chemical reactions are presumed to be fast with respect to the flow's transport processes and combustion is considered to be mixing-limited. The EDM model [20] has been used to compute the mean reaction rate, $\dot{\omega}_k$, Eq. (3). The model can in principle be applied to both premixed and nonpremixed flames. When reactants mix at the molecular level, they instantaneously form products and the reaction rate is related directly to the turbulence mixing time defined by κ and ϵ. The mean reaction rate of the ith species in reaction $\mathbf{r}$ is calculated as:

$$\dot{\omega}_{i,r} = A_{\text{ebu}}\rho\frac{\varepsilon}{\kappa}\min\left[\min_{\text{Reactants}}\left(\frac{\nu'_{i,r}M_iY_R}{\nu'_{R,r}M_R}\right), B_{\text{ebu}}\frac{\nu'_{i,r}M_i\sum_{\text{Products}}Y_P}{\sum_{\text{Products}}\nu''_{P,r}M_P}\right] \tag{16}$$

in which A_{ebu} and B_{ebu} are dimensionless empirical coefficients taken equal to 4.0 and 0.5, respectively.

Coupling the Spalart–Allmaras Model to the Eddy Dissipation Model

As reported earlier, the core of the EDM, as the majority of turbulent combustion models, is based upon the turbulent micromixing time, equal to the ratio of κ to ϵ.

When the SA turbulence model is used, only one turbulence quantity is computed. A second-turbulence quantity must be made available to compute the micromixing time. A natural choice would be the absolute value of the vorticity $|\Omega|$, a quantity which is related to the turbulent production and dissipation rates in most of two-equation turbulence models. Whatever the choice, the sought quantity and the available modified eddy diffusivity $\tilde{\nu}$, when combined together, should be able to provide two new turbulent quantities (κ_{SA} and ϵ_{SA}), which must satisfy two requirements:

1) They should assume any given and arbitrary constant values at inflow boundaries, as form, position, and stability of the flame strongly depend on the turbulence level of the incoming flow.

2) They should have the same wall behavior as the true κ and ϵ.

The choice of using $\tilde{\nu}$ and $|\Omega|$ would lead to: $\kappa_{\text{SA}} \propto \tilde{\nu}|\Omega|$ and to a dissipation rate proportional to $\tilde{\nu}\,\Omega^2$. Such a choice, however, would not satisfy the first requirement: a uniform stream at inlet having zero vorticity. A better choice [21] may be given by:

$$\kappa_{\text{SA}} = \left(\frac{\tilde{\nu}}{l_t}\right)^2 \qquad \epsilon_{\text{SA}} = C_\mu\frac{\kappa_{\text{SA}}}{\tau_t} = C_\mu\frac{\kappa_{\text{SA}}}{d^2/\tilde{\nu}} \equiv C_\mu\frac{\tilde{\nu}^3}{l_t^2 d^2} \tag{17}$$

in which $C_\mu = 0.09$ and $\tau_t = d^2/\tilde{\nu}$ represents the "true" dissipation time scale of the eddy viscosity in the SA one-equation model, with d the distance from the nearest solid boundary. Relation (17) satisfies the second requirement: the turbulent viscosity's wall behavior is similar to that of κ and ϵ_{SA} is constructed in such a way to mimic the true ϵ. The turbulent kinetic energy from Eq. (17) satisfies the first requirement as well. Furthermore, because the turbulent dissipation occurs at very short distances (d) from solid boundaries, if the length scale (d) is replaced by $d = \min(d, l_t)$, then the first requirement is also satisfied by ϵ_{SA} almost everywhere apart from a very thin layer close to solid walls.

This formulation was used by Mulas and Talice [21] for the coupling of the SA turbulence model with the turbulent flame closure model. The problem with this approach is that the value of l_t is generally unknown and it is not feasible to generalize the model to all possible physical and geometrical configurations when using a constant value.

The problem is thus how to go from ν_t or $\tilde{\nu}$ to the turbulent mixing rate ε/k with a more general approach. A possible solution (used in this work) was firstly proposed by Belmrabet et al.[22]. The idea is to reformulate the problem in a quasi-large-eddy simulation (LES) fashion with the assumption of local equilibrium between the production of turbulent kinetic energy and its dissipation ($P_k = \varepsilon$). In this case the turbulent eddy frequency ($\omega = (1/C_\mu)(\varepsilon/k)$) is related to the strain rate using an LES subgrid-scale mixing rate by:

$$\omega = 1/\sqrt{C_\mu}\cdot|S| \tag{18}$$

where

$$|S| = \sqrt{\left(S_{ij} - \tfrac{1}{3}S_{kk}\right)^2} \tag{19}$$

with the mean strain rate S_{ij} defined as:

$$S_{ij} = \frac{1}{2}\cdot\left(\frac{\partial u_i}{\partial x_j} + \frac{\partial u_j}{\partial x_i}\right) \tag{20}$$

This formulation is valid only in regions rather far from the walls. In fact, near a no-slip wall the strong gradients of the dependent variables and the viscous effects on the transport processes are too large. Therefore, a thoughtful consideration needs to be given as to how to make the model suitable in regions close to solid walls. To overcome this problem, a proper wall function (based on a two-layer approach) is used to set both ε and k in the near-wall cells. The computational domain is subdivided into two regions: a viscosity-affected region (near walls) and a fully turbulent region (away from walls). The limit between the two regions is determined by a wall-distance-based, local, turbulent Reynolds number Re_y. The standard coupling (quasi LES model) is used away from the wall ($Re_y > 200$). In the near-wall region ($Re_y < 200$), κ is evaluated from the resolved field variables, whereas l_t is specified by reasonably well-established algebraic equations. As for the turbulence energy equation model, for which two unknown parameters (turbulence length scale, l, and dissipation rate, ε) exist, various methods have been proposed to determine the length scale. Purely dimensional arguments show that $\varepsilon = C_D k^{3/2}/l$ and a number of approaches use length scale distributions similar to those used for the mixing-length model with damping factors (see [11] for more details). Then in the viscosity-affected near-wall region, the ε field is computed from:

$$\varepsilon_{\text{SA}} = \lambda_\varepsilon\cdot(k_{\text{SA}}^{\frac{3}{2}}/l_\epsilon) \tag{21}$$

in which λ_ε is defined in such a way that it is equal to unity far from walls and is zero very close to walls. The chosen λ_ε and l_ε are [23]:

$$\lambda_\varepsilon = 0.5(1 + \tanh\{[Re_y - 200]/[40/\tanh(0.98)]\}) \tag{22}$$

$$l_\varepsilon = y\cdot C_l\cdot(1 - e^{-\frac{Re_y}{A_\varepsilon}}) \tag{23}$$

where

$$C_l = 0.4187\cdot C_\mu^{-0.75} \quad \text{and} \quad A_\varepsilon = 2\cdot C_l$$

The local Reynolds number Re_y is given by the following equation in which y is the distance to the closest wall:

$$Re_y = \left(\sqrt{k_{\mathrm{SA}}} \cdot y\right)/\nu \tag{24}$$

The problem, when using RANS solver, is how to estimate the value of $\varepsilon_{\mathrm{SA}}$ that appears in the κ_{SA} equation given by:

$$k_{\mathrm{SA}} = \sqrt{(\nu_t \cdot \varepsilon_{\mathrm{SA}})/C_\mu} \tag{25}$$

From dimensional analysis ε is generally computed as:

$$\varepsilon = \nu \cdot |\Omega'|^2 \tag{26}$$

in which Ω' is the vorticity fluctuation, whose value is higher than vorticity itself. Indeed, RANS models do not see fluctuating quantities, so that the idea is to evaluate $\varepsilon_{\mathrm{SA}}$ as a function of the resolved field variables. Equation (26) in this case can be rewritten as:

$$\varepsilon_{\mathrm{SA}} = \nu \cdot |\Omega|^2 \tag{27}$$

And finally the inverse of the turbulent mixing time can be computed as:

$$\text{if } \begin{cases} Re_y > 200(\epsilon/k) = \sqrt{C_\mu} \cdot |S| \\ Re_y < 200(\epsilon/k) = \lambda_\varepsilon \cdot (k_{\mathrm{SA}}^{\frac{1}{2}}/l_\varepsilon) \end{cases} \tag{28}$$

Test Cases

Piloted Jet Diffusion Flame of Methane–Air (Masri–Bilger–Dibble)

The suggested SA chemistry coupling is tested against a number of methane–air diffusion flames stabilized by means of a pilot flame. The aim is the investigation of the model's ability, even when coupled with a simple combustion model like the EDM, to provide results in the same range of accuracy as those obtained in previous numerical studies based upon more refined and complex combustion models.

The selected flames have been experimentally studied at the Sandia Turbulence Diffusion Flame Facility [24] using pulsed spontaneous Raman–Rayleigh scattering in the soot free regions. Because of the simplicity of the flow configuration and to the presence of a fully developed turbulent zone in the flame, the proposed test appears to be an ideal test case for the investigation of the interaction between turbulence and chemistry and thus for the development and validation of numerical models [25]. The experimental setup consists of a vertical axisymmetric jet of methane surrounded by an annulus of a completely burned stoichiometric premixed mixture of (C_2H_2, H_2) and air. The complete combustion of this mixture gives products having the same C/H ratio as that of a stoichiometric mixture of methane and air. The flame is then surrounded by a coflow of air blown using a centrifugal fan with adjustable speed. The methane jet temperature is 300 K and it exits from a 7.2 mm-diam pipe ($R = 3.6$ mm), with speed set to 27, 41, and 55 m/s for flames K, L, and M, respectively. The diameter of the external annulus is equal to 18 mm. The speed of the burned gases of the pilot flame is kept at the same level for the three flames and equal to 24 m/s. In all cases, temperature and velocity of the air coflow are 300 K and 15 m/s, respectively. Over the past decade lots of studies have been carried out using different methods to simulate these flames. Some of the most relevant works are summarized hereinafter.

Masri and Pope [26] used a Monte Carlo method. A velocity-composition joint PDF transport equation was used to calculate the flame structure by assuming a constant turbulence frequency Ω (i.e., the turbulent time scale is constant across the flow) and simple reaction scheme. The authors concluded that the model predictions, even with simple thermochemistry, were favorable for slowly mixing flame (flames K and L). Whereas they were considered poor for intensively mixed flame (flame M) because of the occurrence of localized flame extinctions.

Zurbach et al. [27] used a Monte Carlo method coupled with the HADES CFD code (the ESTET-Combustion 2-D version code) to resolve the composition joint PDF transport equation with a reduced chemical kinetics model intrinsic low-dimensional manifold for three flames structures (A, B, and L). The κ–ϵ model was used to close the turbulent convection term in the PDF transport equation. Whereas results for the flames A and L showed a good agreement of the computed mean temperature and mass fractions with experimental measurements; the intermediate concentrations of species and the partial extinction of the flame B were not properly captured.

Saxena and Pope [28] used a Lagrangian particle/mesh method implemented in the PDF2DV code to resolve the joint PDF transport equation with a detailed chemical kinetics using a reaction scheme of 41 reactions and 16 species with the use of the in situ adaptative tabulation algorithm for the effective calculation of the detailed chemistry. They obtained better results for minor species compared with those of Zurbach et al. [27]. The mean temperature, however, is overpredicted throughout and mainly on the side of the coflow ($r/R > 3$), as mentioned by the authors. Their explanation for this behavior is related to the fact that the model is extremely sensitive to errors in the mixture fraction evaluation.

The present computation has been carried out over a 5-deg sector of the flame, taking advantage of the flow's periodicity. Figure 1 visualizes the main geometrical features and boundary conditions used for the computation. The structured computational domain consists of some 24,400 cells ($177 \times 46 \times 3$ grid points). An implicit total variation diminishing (TVD) second-order scheme has been used with a CFL number of 20. Profiles of velocity and turbulent viscosity [26] have been assigned as inlet conditions.

Figure 2 shows the convergence's history of normalized residuals of momentum, eddy viscosity, and species.

To assess the grid independency of the computed results, computation has been repeated on a finer grid ($353 \times 91 \times 3$ grid points). Figure 3 compares profiles of normalized density between

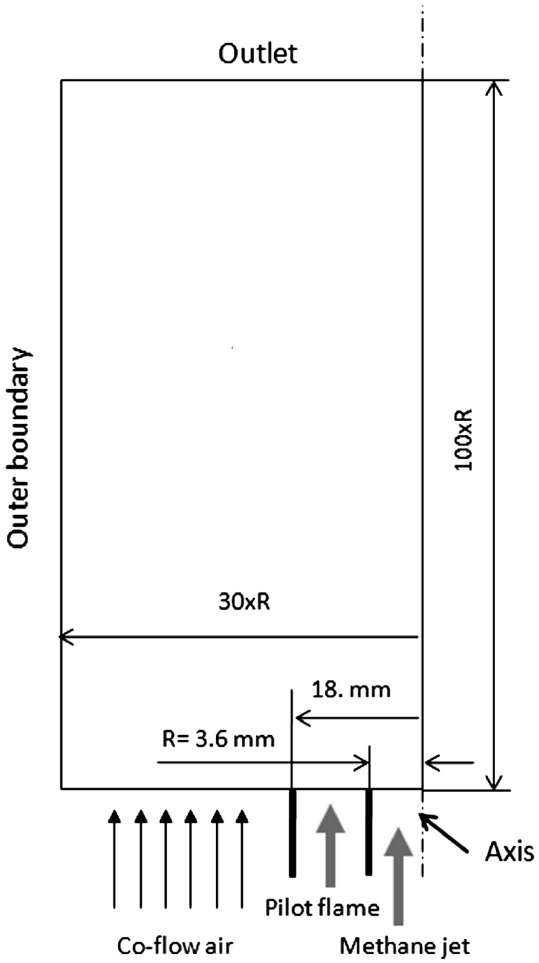

Fig. 1 Sketch of the Masri flame computational domain.

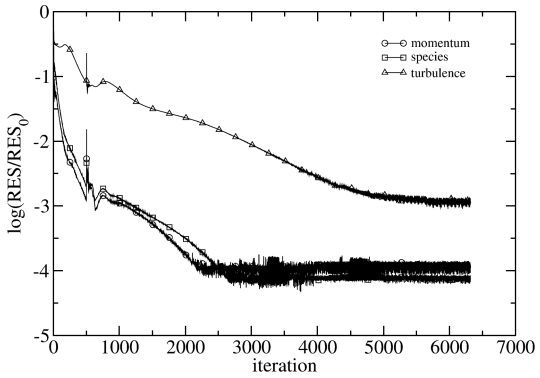

Fig. 2 Convergence's history of normalized residuals of momentum, viscosity, and species.

coarse and fine grids. Solutions are substantially close to each other and the coarse grid has been then used to run all the simulations.

Results are compared with experimental data of Masri et al. [24] at various axial locations for K, L, and M flames. Because of the plethora of numerical studies devoted to flame L, special attention is paid to this flame. Comparison with numerical results of Zurbach et al. [27], Masri and Pope [26], and of Saxena and Pope [28], is also offered. All the cited previous numerical studies have been carried out with PDF-based turbulent combustion models. To establish baseline results and to provide a better evaluation of the method of determining the mixing time, simulation of flame L is repeated by using the κ-ϵ turbulence model coupled with the EDM combustion model. The κ-ϵ model's coefficients have been recalibrated for axisymmetric flows, as suggested in [29].

Velocity and Density Fields

Figures 4–6 show radial profiles of normalized axial velocity at two locations along the burner for the three flames K, L, and M,

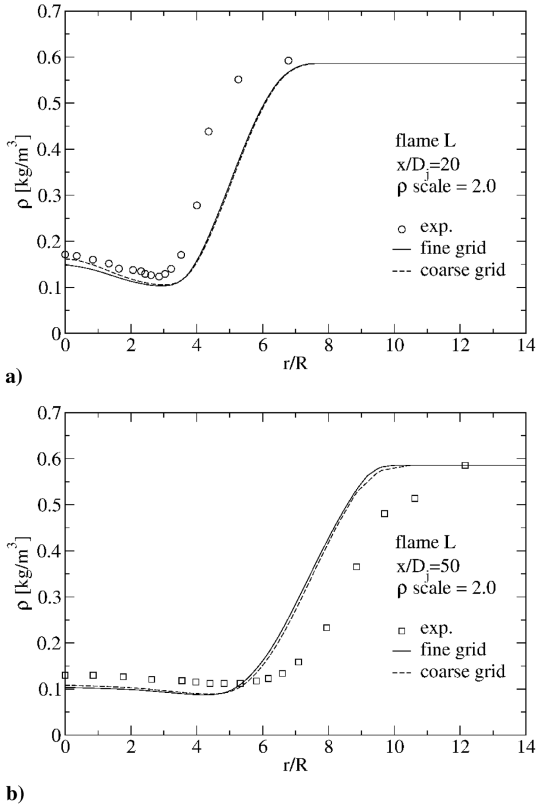

Fig. 3 Assessment of solution's grid independency: radial profile of normalized axial velocity at a) $x/D = 20$ and b) $x/D = 50$. Comparison with experimental data [24].

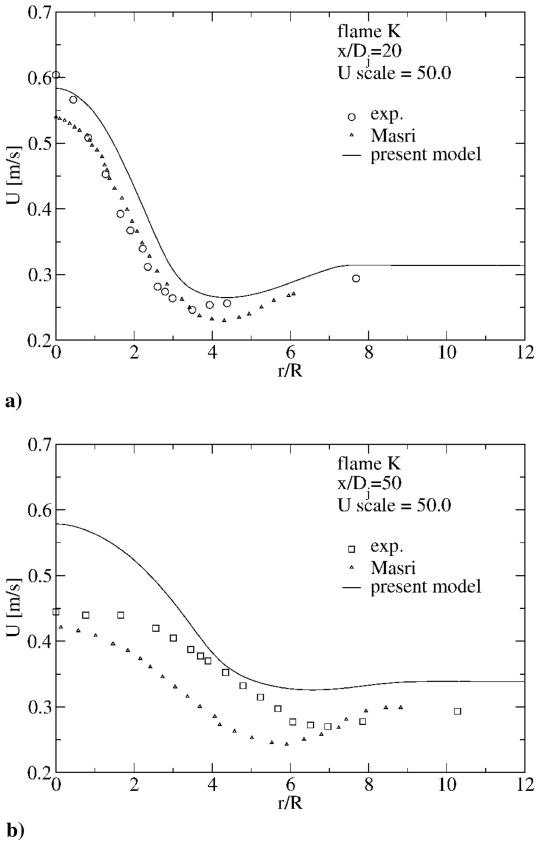

Fig. 4 Radial profile of normalized axial velocity at: a) $x/D = 20$ and b) $x/D = 50$. Comparison with experimental data [24] and numerical results [26].

respectively. At $x/D = 20$, the overall agreement with experimental data is fairly good and the curve's slope is generally well captured. Far from the centerline of the burner, numerical results are higher than experimental values by about 7, 5 and 13% for flames K, L, and M respectively and the error reduces for $r/R > 5$. The general overestimation of velocity is probably due to two main factors, whose relative weight is different at different spatial locations. In the proximity of the burner's centerline, until about $r/R < 3$, the leading error can be related to an insufficient resolution of turbulence in this zone, or to the influence of the turbulence boundary conditions used at the inlet section. In fact, the inlet profile of turbulent viscosity has been calculated from the measured data of velocity's fluctuation and from an estimated turbulent integral scale, taken as a function of the burner's radius for $r/R < 1$ and fixed to a constant value for $r/R > 1$. To investigate the sensitivity of results to the inlet turbulence boundary conditions, computation has been repeated with three different values of the turbulent integral scale. The computed velocity profiles at $x/D = 20$ are shown in Fig. 7. Examination of Fig. 7 shows that the turbulent integral scale is correctly specified as multiplication or division of the chosen value by a factor of 10 (in the zone of $1 < r/R < 3$), does not significantly change the computed results. For $r/R > 3$, the overestimation of temperature (see Figs. 8 and 9) and the subsequent underestimation of density (see Figs. 10 and 11) seems to be the most likely factor that determines the velocity's overprediction.

In the vicinity of the burner's centerline, velocity predicted by Masri and Pope [26] is about 10% lower than experimental data. Prediction obtained with the κ–ϵ–EDM model (flame L only) shows a fairly good agreement with the experimental data over the entire range of r/R. At $x/D = 50$, both the present model and the κ–ϵ–EDM model overshoot measurements, whereas results obtained by Masri and Pope [26] tend to underestimate the experimental data. At this section it is found that errors increase as the fuel injection velocity is augmented. This can be due to an incorrect estimation of

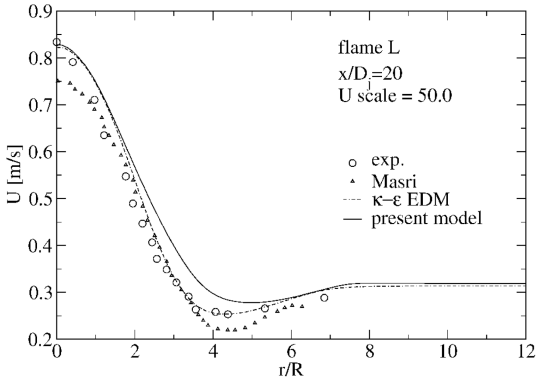

a)

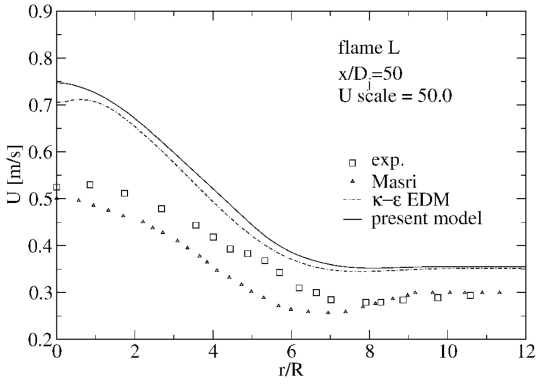

b)

Fig. 5 Radial profile of normalized axial velocity at: a) $x/D = 20$ and b) $x/D = 50$. Comparison with experimental data [24] and numerical results [26]. Results obtained with κ–ϵ–EDM model are also reported.

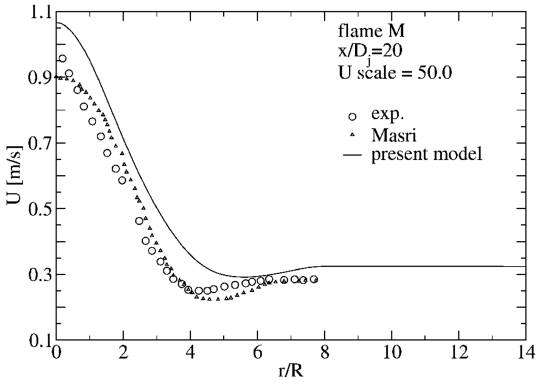

a)

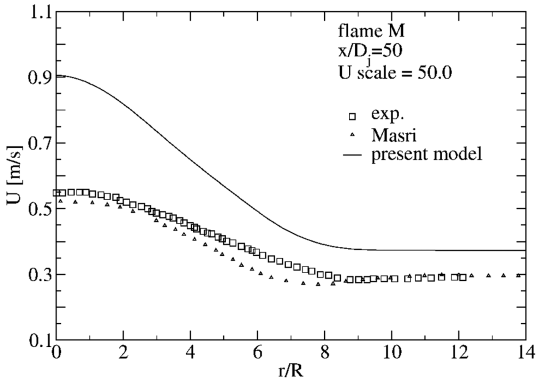

b)

Fig. 6 Radial profile of normalized axial velocity at: a) $x/D = 20$ and b) $x/D = 50$. Comparison with experimental data [24] and numerical results [26].

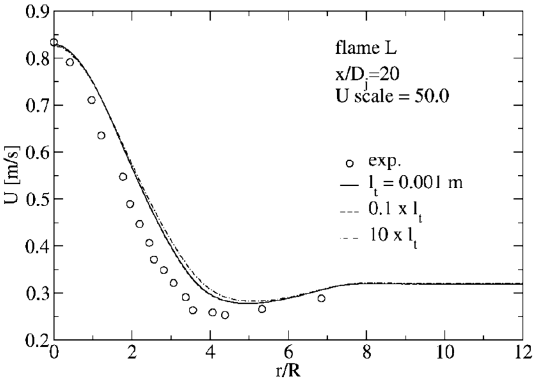

Fig. 7 Solution's sensitivity to inlet conditions, velocity profile at $x/R = 20$, for three different values of turbulence length scale.

turbulence or a consequence of a too-high thermal expansion caused by the temperature's overprediction.

Radial profiles of normalized density for the three flames are shown in Figs. 10 and 11. At $x/D = 20$, density appears well captured for flames K and L, especially in the region of $r/R < 3$ in which the present results fit the experimental data better than those of Masri and Pope [26], overestimating measurements for $r/R < 1$ and underestimating them for $1 < r/R < 3$. In turn, Masri's results approximate better the experimental profile for $r/R > 3$. The κ–ϵ–EDM model is shown to provide good prediction also in the region of $r/R > 3$. For flame M, the density's profile is not well captured. This is probably due to the high intensity of the mixing rate in this zone caused by the high jet velocity [26], inducing local extinctions. The combustion model used in this work is not able to detect this kind of phenomena. At $x/D = 50$, an overall satisfactory agreement is obtained except for flame M, for which density is again

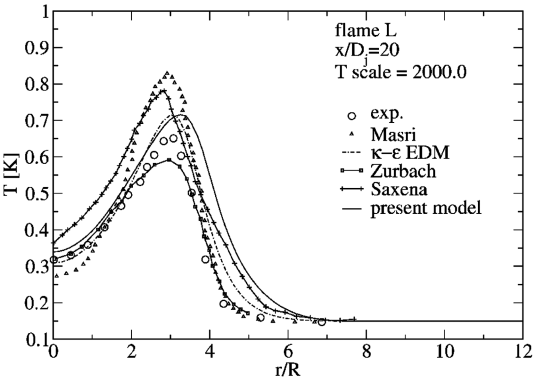

a)

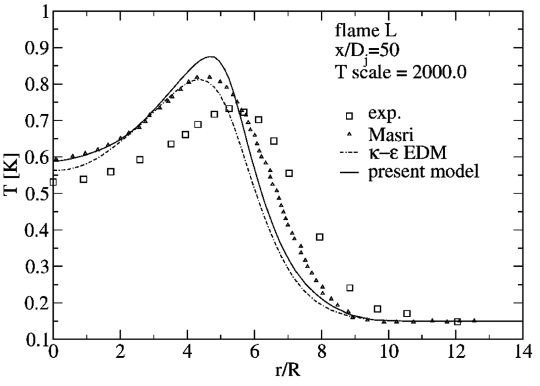

b)

Fig. 8 Radial profile of normalized temperature at: a) $x/D = 20$ and b) $x/D = 50$. Comparison with experimental data [24] and numerical results [26–28] ($x/d = 20$ only). Results obtained with κ–ϵ–EDM model are also reported.

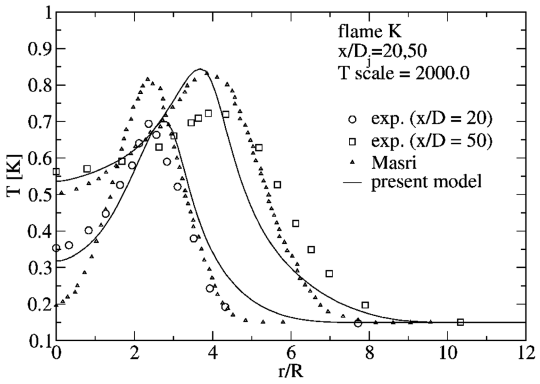

a)

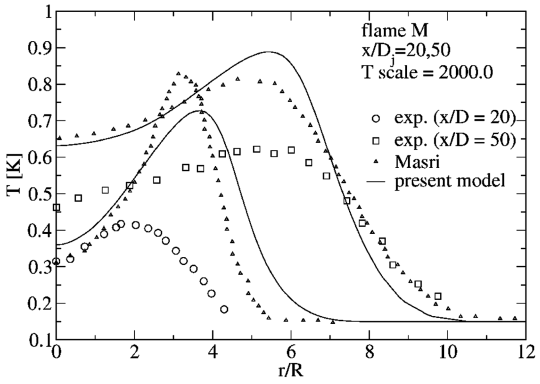

b)

Fig. 9 Radial profile of normalized temperature for flame: a) K and b) M. Comparison with experimental data [24] ($\bigcirc$ $x/D = 20$, $\square$ $x/D = 50$) and numerical results [26].

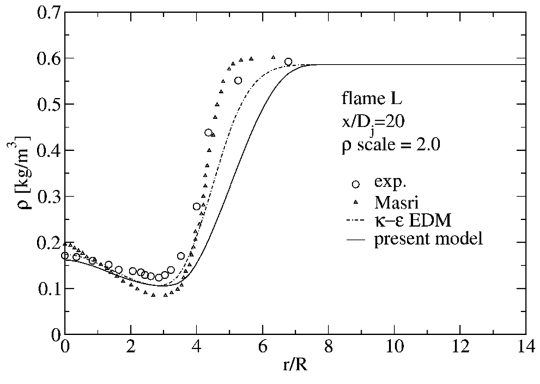

a)

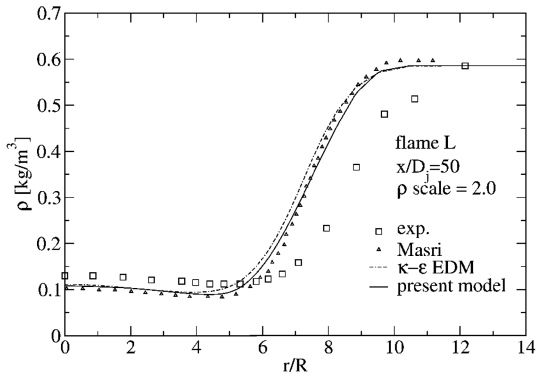

b)

Fig. 10 Radial profile of normalized density at: a) $x/D = 20$ and b) $x/D = 50$. Comparison with experimental data [24] and numerical results [26]. Results obtained with κ–ϵ–EDM model are also reported.

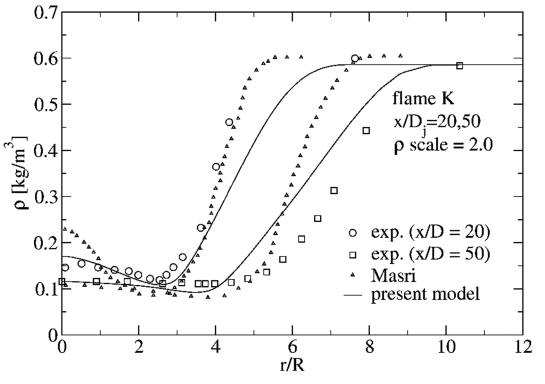

a)

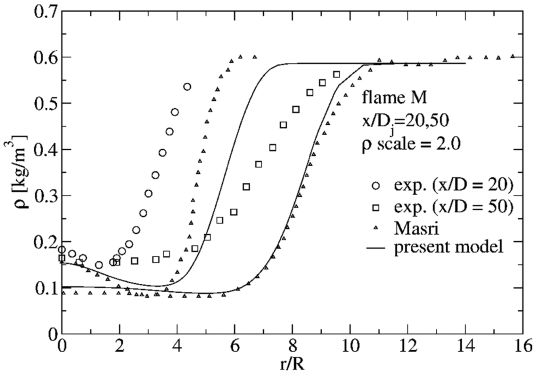

b)

Fig. 11 Radial profile of normalized density for flame: a) K and b) M. Comparison with experimental data [24] ($\bigcirc$ $x/D = 20$, $\square$ $x/D = 50$) and numerical results [26].

underpredicted. The same level of accuracy is also obtained by Masri and Pope [26].

Temperature Field

Comparisons of predicted and measured radial normalized mean temperature profiles for the three flames at two axial locations are shown in Figs. 8, 9, and 12. At $x/D = 20$, a good agreement with measurements is obtained for flames K and L. Figure 8 in particular, shows that, although amplitude and position of the temperature's peak are both overpredicted, the present model is able to provide results in good agreement with experiments for low values of r/R, and in the same range of accuracy as other numerical results as the radius increases. The proposed model shows an error of about 40 and 300 K at $x/D = 20$ and $x/D = 50$, respectively. The κ–ε–EDM model shows the same temperature overprediction as the proposed model at $x/D = 20$; but the temperature's peak position is more correctly captured. At $x/D = 50$ the temperature overprediction is of about 250 K. At $x/D = 20$ results of Zurbach et al.[27] better approximate the experiments, whereas Masri and Pope's [26] and Saxena and Pope's [28] results overshoot the temperature's peak by some 400 and 250 K, respectively. Saxena's results suggest that the use of detailed chemistry coupled with the JPDF approach seem not to be sufficient to guarantee good temperature's predictions, even if better results in terms of minor species concentrations can be found, as will be explicitly considered later. For flame M the obtained temperature's peak is higher than the measured one by about 650 K, which is in the same level of agreement as Masri and Pope's results [26], who obtained an overprediction of mean temperature's peak of about 850 K. The measured temperature's peaks are of about 1400, 1300, and 800 K for flames K, L, and M, respectively. The low temperature's value for flame M in this zone, characterized by high mixing intensity, is experimentally found [24] to be due to local extinctions. As was mentioned earlier, the combustion model is not able to capture this phenomenon. At $x/D = 50$ the measured temperature's peak for flame M reaches 1205 K, which indicates that

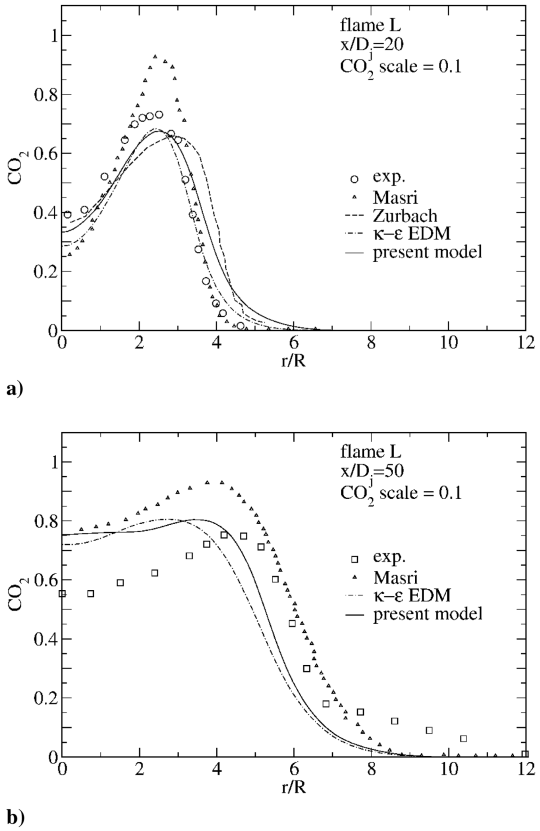

Fig. 12 Radial profile of normalized CO_2 concentration at: a $x/D = 20$ and b) $x/D = 50$. Comparison with experimental data [24] and numerical results [26,27]. Results obtained with κ–ϵ–EDM model are also reported.

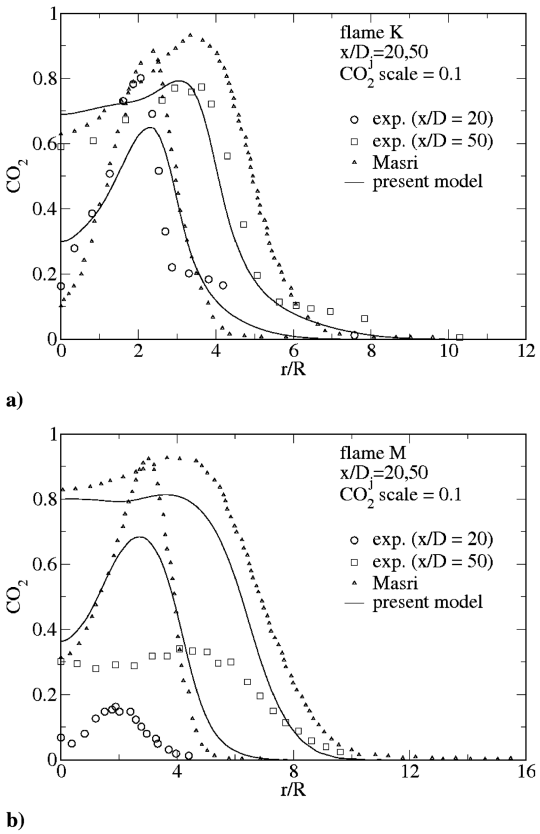

Fig. 13 Radial profile of normalized temperature for flame: a) *K* and b) *M*. Comparison with experimental data [24] (○ $x/D = 20$, □ $x/D = 50$) and numerical results [26].

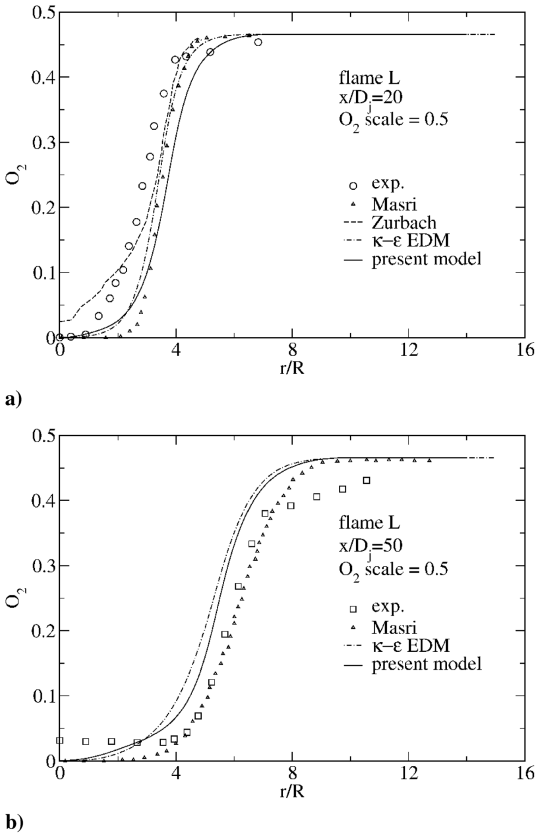

Fig. 14 Radial profile of normalized O_2 concentration at: a) $x/D = 20$ and b) $x/D = 50$. Comparison with experimental data [24] and numerical results [26,27]. Results obtained with κ–ϵ–EDM model are also reported.

reignition has occurred further downstream in which the mixing intensity is reduced. An acceptable level of agreement with measurements is obtained in this zone for the three flames. The predicted temperature's peak in flame *M* is higher than the measured one by about 500 K. This overprediction reduces to some 300 K for flames *K* and *L*.

Species Concentration

Normalized radial profiles of carbon dioxide CO_2 and oxygen O_2 for the three flames are shown in Figs. 12–15. The results' quality is similar to those obtained for temperature. For flames *K* and *L*, a good agreement with experiments at $x/D = 20$ and an acceptable level of agreement at $x/D = 50$ is shown. All computed results do not look good for flame *M*, especially in the zone of high mixing intensity ($x/D = 20$) in which extinction occurs. At $x/D = 50$, the radial profile of oxygen is poorly captured. The predicted value of the oxygen's mass fraction is about zero at the centerline whereas the measured value is equal to 0.117. These results show once again the inability of the models to simulate this type of flame. Figure 16 shows radial profiles of carbon monoxide CO for flame *L* at two axial locations ($x/D = 20$ and 30). A substantial difference between predicted values and measurements can be observed. The predicted peak value of CO's mass fraction is in fact lower than the measured one by about 50%. The same level of accuracy is obtained by Zurbach et al. [27] and by the κ–ε–EDM model. Saxena and Pope's results [28] show a good agreement with measurements; but the global flame structure is not well captured as observed earlier while commenting on temperature profiles.

Moreau Combustor

The second test, experimentally studied by Moreau [30] and Moreau and Borghi [31], simulates a turbulent premixed flame in a combustion chamber of rectangular cross section. The test case is

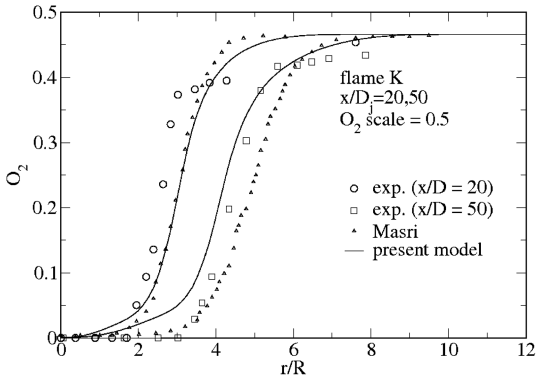

a)

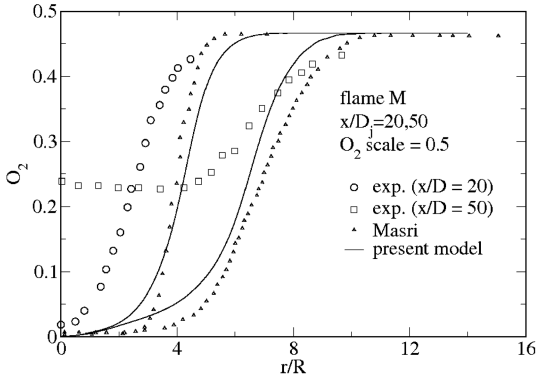

b)

Fig. 15 Radial profile of normalized temperature for flame: a) *K* and b) *M*. Comparison with experimental data [24] (○ $x/D = 20$, □ $x/D = 50$) and numerical results [26].

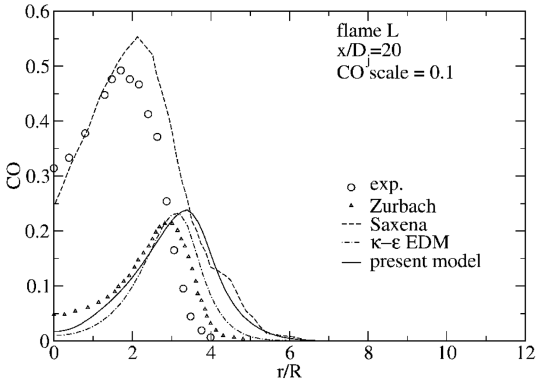

a)

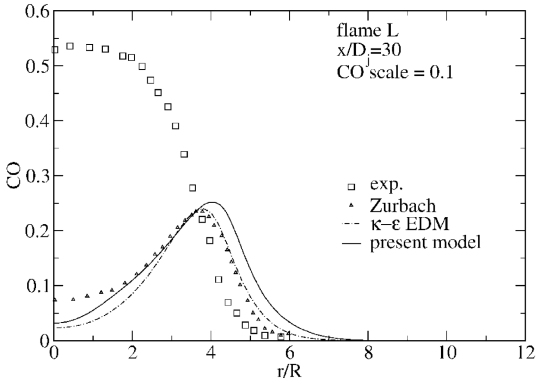

b)

Fig. 16 Radial profile of normalized CO concentration at: a) $x/D = 20$ and b) $x/D = 30$. Comparison with experimental data [24] and numerical results [27,28] ($x/D = 20$ only). Results obtained with κ–ϵ–EDM model are also reported.

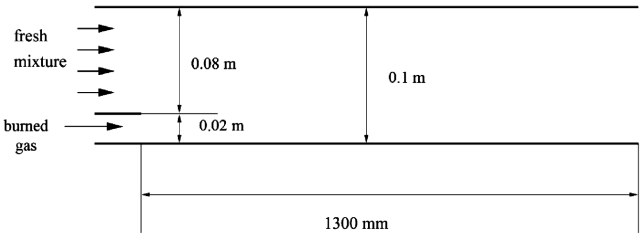

Fig. 17 Moreau's combustor: geometrical configuration and flow conditions.

somewhat representative of a typical industrial burner. Results have been compared with both experimental data and numerical results of Benin and Syed [32], who made use of this test case to validate a laminar flamelet method. The duct combustor has a rectangular cross section as described in Fig. 17. Though turbulence is inherently three-dimensional, due to the high aspect ratio of the duct cross section, three-dimensional effects induced on the flow by the side walls boundary layers can be neglected (2-D planar channel) when the combustor's midspan section is taken into account. The fresh mixture, after being forced throughout a turbulator to enhance its turbulence level, enters the left upper part of the combustor and is ignited and stabilized by a coflowing fully turbulent stream of high temperature exhaust gases resulting from complete combustion of a methane–air mixture in an auxiliary burner located upstream. Both streams are then fully turbulent and values for mean velocity and turbulence intensity can be used to specify inlet conditions, without the need to assume any inlet boundary-layer profile. Heat transfer from the hot burned mixture to the fresh mixture across the mixing layer that separates the two streams can cause ignition. Grid distribution at this interface is adapted in such a way as to capture the heat and mass turbulent diffusion. In fact, the hot stream is used to anchor the flame by providing a continuous source of heat, whereas the fresh stream is considered fully premixed already. The use of fast chemistry assumption makes the determination of the exact position of the flame's stabilization point impossible, because the EDM model lacks of the ignition mechanism, which involves complex chemistry [1]. The composition of the hot stream of gases is assumed to correspond at the equilibrium status for the fixed temperature of 2000 K, which is rather low despite an equivalence ratio equal to unity. This could be due to heat losses in the pilot burner. The composition of the burnt fuel-air mixture is assumed to correspond to adiabatic equilibrium conditions [33]. An implicit TVD second-order scheme has been used with a CFL number of 100. Pressure and temperature of the fresh mixture are 1 bar and 600 K, respectively. Table 1 summarizes the mixture composition and the flow's conditions at the two inlets.

Computations have been carried out on a grid of some 14,000 cells (106×129 grid points). Computations have been repeated on a finer grid (211×257 grid points) to assess the results' grid independence. Figure 18 shows profiles of temperature at two locations along the combustor for coarse and fine grids. Results show a substantial grid independence. Only results on the coarse grid are presented for

Table 1 Inlet conditions

	Fresh mixture	Burned mixture
u, m/s	57	112
v, m/s	0	0
T, K	600	2000
κ, m^2/s^2	63.375	174.96
Turbulence intensity	13%	4.5%
l_t, m	5.6×10^{-3}	1.4×10^{-3}
$\tilde{\nu}$, m^2/s	4.4581×10^{-2}	1.8518×10^{-2}
Φ	0.83	1.0
Y_{CH_4}	0.04620	0.0
Y_{O_2}	0.22206	0.0
Y_{CO_2}	0.0	0.1258
Y_{H_2O}	0.0	0.1225

velocity and oxygen concentration and will be referred to as "present model" in the following figures. The overall agreement with the experimental data [30,31] and numerical results [32] is fairly good. Examination of Fig. 18 shows that the correct slope is well captured by the computation. At the first section ($x = 322$ mm), in which the temperature's gradients are high, the model provides a general overprediction of temperature over most of the curve. This can be due to the incorrect value of the boundary values of temperature and composition of the pilot flame. At the second section ($x = 922$ mm), localized near the burner's outlet, a fairly good agreement between prediction and experiment can be observed. Although the curve's slope is well captured, results still show an overprediction of temperature over most of the combustor's span. It is well known that the EDM model tends to overestimate the peak mean temperature values, as found in the present work. Near the walls, temperature is underpredicted, but higher than those obtained by Benin and Syed [32]. Moreau [30] and Moreau and Borghi [31] do not provide any measurements for the walls' temperature, so that adiabatic wall conditions are assumed. In his computations Benin and Syed [32] fixed wall temperature at 600 K.

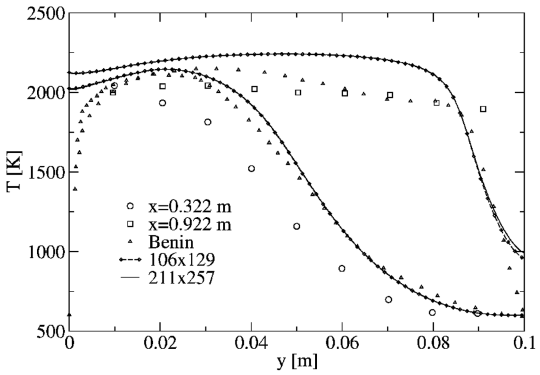

Fig. 18 Temperature's profiles at $x = 0.322$ and $x = 0.922$ m.

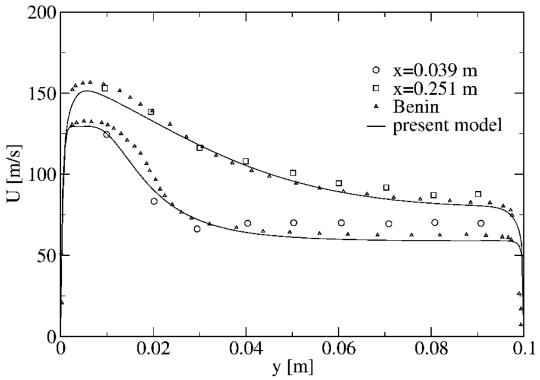

Fig. 19 Axial velocity's profiles at $x = 0.039$ and $x = 0.251$ m.

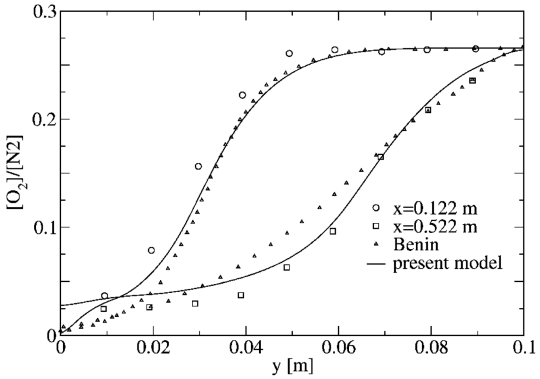

Fig. 20 Profiles of normalized O_2 concentrations at sections $x = 0.122$ and $x = 0.522$ m.

Transverse profiles of the axial velocity in Fig. 19 reveal an overall good agreement with experimental and numerical data at all locations. The curve's slope is generally well captured. At the first section, experiments show an abrupt variation in the velocity's profile close to the region in which the shear layer is present (due to the different velocity values at the combustor's inlet). The velocity gradient is correctly captured using the proposed model. Beyond this zone, results show an underprediction of the axial velocity. This can be due either to an insufficient resolution of the turbulent behavior of the flow in this zone, or a consequence of the temperature's overprediction mentioned earlier. At the second section, the correct velocity profile is generally well captured. The axial velocity is increased by thermal expansion of combustion products and the abrupt variation vanishes.

Figure 20 depicts the comparison of the computed transverse profiles of normalized oxygen's mass fraction with experimental and numerical data. At both locations, the oxygen's profiles are well captured.

Conclusions

The extension of a preconditioned CFD solver to the analysis of both diffusive and premixed turbulent flames was presented. The method is based on the use of a fully compressible formulation with matrix numerical dissipation (Roe's scheme) and the SA one-equation turbulence model. The Roe's scheme is applied to the coupled system of mass, momentum, energy, and species equations, and the solution is advanced in time by an implicit method. The Message Passing Interface parallel environment allows the use of an arbitrary number of processors for the simulation of realistic 3-D combustors. One of the key issues addressed in the paper is the derivation of an accurate and consistent turbulent time field out of the only turbulent resolved quantity, namely, the SA eddy diffusivity. The methodology has been used in conjunction with the simple EDM combustion model, but it can be used with any other model requiring the determination of the turbulent time field. The two test cases presented, the premixed Moreau combustor and the Masri unconfined diffusive flame, both showed results that compare well with experiments and previous numerical studies. The present work demonstrates that the turbulent combustion analysis maintains the well-known accuracy, robustness, and generality of the method (preconditioned Roe's scheme and SA model) when applied to nonreactive flows. Future work will focus on coupling the SA model with other combustion models and on the implementation of the proposed methodology in a delayed-detached eddy simulation (DDES) framework. In addition to that, the new method will be tested against a class of transonic and supersonic reactive flows.

References

[1] Poinsot, T., and Veynante, D., *Theoretical and Numerical Combustion*, R. T. Edwards, Philadelphia, 2001, pp. 202–231, 292–308.

[2] Spalding, D. B., "Development of the Eddy-Break-up Model of Turbulent Combustion," *Sixteenth Symposium (International) on Combustion*, Combustion Inst., Pittsburgh, PA, 1976, pp. 1657–1663.

[3] Moss, J. B., and Bray, K. N. C., "A Unified Statistical Model of the Premixed Turbulent Flame," *Acta Astronautica*, Vol. 4, No. 3–4, 1977, pp. 291–319.
doi:10.1016/0094-5765(77)90053-4

[4] Borghi, R., "Critiques sur la Modelisation de la Combustion Turbulente," *Proceedings of the Symposium, Sophia-Antipolis*, *Lecture Notes in Physics*, Vol. 241 Springer–Verlag Berlin May 1985, pp. 20–31.
doi:10.1007/BFb0008648

[5] Maistret, E., Darabiha, N., Poinsot, T., Veynante, D., Lacas, F., Candel, S., and Esposito, E., "Recent Developments in the Coherent Flamelet Description of Turbulent Combustion," *Proceedings of the Third International Conference on Numerical Combustion, Juan les Pins, Antibes*, *Lecture Notes in Physics*, Vol. 351, Springer–Verlag, New York,

May 1989, pp. 98–117.
doi:10.1007/3-540-51968-8_78
[6] Duclos, J. M., Veynante, D., and Poinsot, T., "A Comparison of Flamelet Models for Premixed Turbulent Combustion," *Combustion and Flame*, Vol. 95, Nos. 1–2, 1993, pp. 101–117.
doi:10.1016/0010-2180(93)90055-8
[7] Mantel, T., and Borghi, R., "A New Model of Premixed Wrinkled Flame Propagation Based on a Scalar Dissipation Equation," *Combustion and Flame*, Vol. 96, No. 4, 1994, pp. 443–457.
doi:10.1016/0010-2180(94)90110-4
[8] Cheng, W. K., and Diringer, J. A., "Numerical Modelling of SI Engine Combustion with a Flame Sheet Model", Society of Automotive Engineers, Paper 910268, 1991.
[9] Marble, F. E., and Broadwell, J. E., "The Coherent Flamelet Model for Turbulent Chemical Reactions," Purdue Univ. TRW-9-PU, West Lafayette, IN,1977.
[10] Veynante, D., and Vervish, L., "Turbulent Combustion Modeling," *Progress in Energy and Combustion Science*, Vol. 28, No. 3, 2002, pp. 193–266.
doi:10.1016/S0360-1285(01)00017-X
[11] Wilcox, D. C., *Turbulence Modeling for CFD*, 2nd_ed, DWC Industries, La Canada, CA, 1994, pp. 73–82.
[12] Spalart, P. R., and Allmaras, S. R., "A One-Equation Turbulence Model for Aerodynamics Flows," AIAA Paper 92-0439, 1992.
[13] Fox, R. O., *Computational Models for Turbulent Reacting Flows*, Cambridge Univ. Press, Cambridge, England, UK, 2003, pp. 114–120.
[14] Mulas, M., Chibbaro, S., Delussu, G., Di Piazza, I., and Talice, M., "Efficient Computations of Flows of Arbitrary Fluids for All Regimes of Reynolds, Mach, and Grashof Numbers," *International Journal of Numerical Methods for Heat & Fluid Flow*, Vol. 12, No. 6, 2002, pp. 637–657.
doi:10.1108/09615530210438337
[15] Bird, R. B., Warren, E. S., and Edwin, N. L., *Transport Phenomena*, 2nd ed., Wiley, New York, 2002, Chaps. 1, 9, 17.
[16] Roe, P. L., "Approximate Riemann Solvers, Parameters Vectors, and Difference Schemes," *Journal of Computational Physics*, Vol. 43, No. 2, 1981, pp. 357–372.
doi:10.1016/0021-9991(81)90128-5
[17] Hirsch, C., *Numerical Computation of Internal and External Flows*, 2nd ed., Wiley, New York, 2007, Chap. 8.
[18] Deck, S., Duveau, P., d'Espiney, P., and Guillen, P., "Development and Application of Spalart–Allmaras One Equation Turbulence Model to Three-Dimensional Supersonic Complex Configurations," *Aerospace Science and Technology*, Vol. 6, No. 3, 2002, pp. 171–183.
doi:10.1016/S1270-9638(02)01148-3
[19] Dacles-Mariani, J., Zilliac, G. G., Chow, J. S., and Bradshaw, P., "Numerical/Experimental Study of a Wingtip Vortex in the Near Field," *AIAA Journal*, Vol. 33, No. 9, 1995, pp. 1561–1568.
doi:10.2514/3.12826
[20] Magnussen, B. F., and Hjertager, B. H., "On Mathematical Modeling of Turbulent Combustion with Special Emphasis on Soot Formation and Combustion," *Sixteenth Symposium (International) on Combustion*, Combustion Inst, Pittsburgh, PA, 1976, pp. 719–729.
[21] Mulas, M., and Talice, M., "Fully Compressible Simulation of Low-Speed Premixed Reacting Flows," AIAA, June 2003, Paper 2003-4253.
[22] Belmrabet, T., Talice, M., Delussu, G., and Hanchi, S., "An Implicit Parallel Fully Compressible Roe Based Solver for Subsonic and Supersonic Reacting Flows," *Proceedings of the ICCFD5 Conference*, *Computational Fluid Dynamics*,Springer–Verlag, Berlin, July 2008.
doi:10.1007/978-3-642-01273-0_19
[23] Chen, C. J., and Patel, V. C., "Near-Wall Turbulence Models for Complex Flows Including Separation," *AIAA Journal*, Vol. 26, No. 6, 1988, pp. 641–648.
doi:10.2514/3.9948
[24] Masri, A. R., Bilger, R. W., and Dibble, R. W., "Turbulent Nonpremixed Flames of Methane Near Extinction: Mean Structure from Raman Measurements," *Combustion and Flame*, Vol. 71, No. 3, 1988, pp. 245–266.
doi:10.1016/0010-2180(88)90062-4
[25] Masri, A. R., Dibble, R. W., and Barlow, R. S., "The Structure of Turbulent Nonpremixed Flames Revealed by Raman–Rayleigh–LIF Measurements," *Progress in Energy and Combustion Science*, Vol. 22, No. 4, 1996, pp. 307–362.
doi:10.1016/S0360-1285(96)00009-3
[26] Masri, A. R., and Pope, S. B., "PDF Calculations of Piloted Turbulent Nonpremixed Flames of Methane," *Combustion and Flame*, Vol. 81, No. 1, 1990, pp. 13–29.
doi:10.1016/0010-2180(90)90066-Z
[27] Zurbach, S., Garreton, D., and Kanniche, M., "Validation of a Monte Carlo Method Using a Joint PDF of the Composition and an ILDM Kinetic Model for the Prediction of Turbulent Flames," *Collection de Notes Internes de la Direction des Études et Recherches*, Electricite de France EDF-DER-98 NB00006, Clamart, France, 1998.
[28] Saxena, V., and Pope, S. B., "PDF Calculation of Major and Minor Species in a Turbulent Piloted Jet Flame," *In Twenty-Seventh Symposium (International) on Combustion*, Combustion Inst., Pittsburgh, PA, 1998, pp. 1081–1086.
[29] Turpin, G., and Troyes, J., "Validation of a Two-Equation Turbulence Model for Axisymmetric Reacting and Non-Reacting Flows," AIAA Paper 00-3463, 2000.
[30] Moreau, P., "Turbulent Flame Development in a High Velocity Premixed Flow," ONERA, T.P. 1977-5, Hauts-de-Seine, France, 1977.
[31] Moreau, P., and Borghi, R., "Experimental and Theoretical Studies of Nitrogen Oxides Production in a Turbulent Premixed Flame," ONERA, T.P. 1980-1, Hauts-de-Seine, France, 1980.
[32] Benim, A. C., and Syed, K. J., "Laminar Flamelet Modelling of Turbulent Premixed Combustion," *Applied Mathematical Modelling*, Vol. 22, Nos. 1–2, Jan.–Feb. 1998, pp. 113–136.
doi:10.1016/S0307-904X(98)00012-2
[33] Zimont, V. L., Biagioli, F., and Khawar, S., "Modeling Turbulent Premixed Combustion in the Intermediate Steady Propagation Regime," *Progress in Computational Fluid Dynamics*, Vol. 1, No. 1, 2001, pp. 14–28.
doi:10.1504/PCFD.2001.001467

K. Anderson
Associate Editor